Phys. Status Solidi RRL **10**, No. 5, 381–387 (2016) / **DOI** 10.1002/pssr.201600004

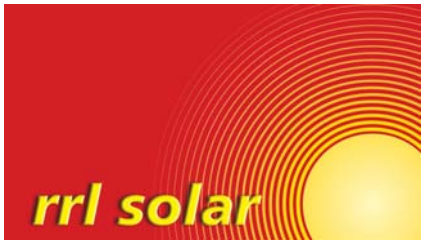

Humidity controlled crystallization of thin $CH_3NH_3PbI_3$ films for high performance perovskite solar cell

Beomjin Jeong[1], Suk Man Cho[1], Sung Hwan Cho[1], Ju Han Lee[1], Ihn Hwang[1], Sun Kak Hwang[1], Jinhan Cho[2], Tae-Woo Lee[3], and Cheolmin Park[*,1]

[1] Department of Materials Science and Engineering, Yonsei University, 50 Yonsei-ro, Seodaemun-gu, Seoul 03722, Republic of Korea
[2] Department of Chemical and Biological Engineering, Korea University, 145 Anam-ro, Seongbuk-gu, Seoul 02841, Republic of Korea
[3] Department of Materials Science and Engineering, Pohang University of Science and Technology (POSTECH), 77 Cheongam-ro, Nam-gu, Pohang, Gyeongbuk 37673, Republic of Korea

Received 11 January 2016, revised 31 March 2016, accepted 31 March 2016
Published online 7 April 2016

Keywords perovskites, solar cells, humidity, crystallization, single crystals, $CH_3NH_3PbI_3$

[*] Corresponding author: e-mail cmpark@yonsei.ac.kr, Phone: +82 2 2123 2833, Fax: +82 2 312 5375

Control of crystallization of a solution-processed perovskite layer is of prime importance for high performance solar cells. In spite of the negative effect of water on perovskite solar energy conversion in several previous works, we observed that humidity plays a critical role to develop a thin uniform, dense perovskite film with preferred crystals, in particular, in a device with architecture of ITO/PEDOT:PSS/$CH_3NH_3PbI_3$/$PC_{71}BM$/LiF/Al fabricated by two-step sequential spin-coating process. Humidity controlled spin-coating of CH_3NH_3I on the pre-formed PbI_2 layer was the most influential process and systematic structural investigation as a function of humidity revealed that grains of $CH_3NH_3PbI_3$ perovskite crystals increase in size with their preferred orientation while film surface becomes roughened as the humidity increases. The performance of a device was closely related to the humidity dependent film morphology and in 40% relative humidity, the device exhibited the maximum power conversion efficiency of approximately 12% more than 10 times greater than that of a device fabricated at 20% humidity. The results suggest that our process with controlled humidity can be another efficient route for high performance and reliable perovskite solar cells.

1 Introduction Recent technological progress in organic–inorganic hybrid perovskite solar cell has shown its great potential for the commercialization as high performance next generation solar cell due to its outstanding photovoltaic properties [1–3]. Solution processibility of a thin perovskite film such as spin-coating is additionally beneficial, making this solar cell cost-effective. To ensure high energy conversion efficiency, numerous previous works have devoted to understanding mechanisms of thin perovskite film formation based on nucleation and growth of crystals and thus to develop structurally dense and uniform film with properly grown crystals [1–19]. In particular, control of crystallization of a perovskite layer in recently prevailing one or two-step solution-processed solar cell is one of the most important issues for guaranteeing high performance. Since spin-coating frequently used for film formation involves extremely rapid solvent evaporation, the growth dynamics of the film involving strong ionic interactions between the metal cations and halogen anions are rarely understood, making it difficult to control the crystallization. In fact, depending not only on the processing conditions but also on the lead halides, the crystalline orientation, grain shape and size of the resulting perovskite layer were largely varied.

Control of a thin crystalline perovskite film is even more difficult in one-step spin-coating method in which micron-sized needle crystals or highly rough crystals are often developed with undesirable pinholes in films. Special

cares should be, therefore, taken to avoid high leakage and shunting paths and thus improve the device performance but these additional treatments render the fabrication processes more complicated [4–9]. On the other hand, two-step sequential spin-coating process is beneficial in a sense that crystallization of perovskite film can be more systematically examined in two separate steps [10]. In two-step spin-coating process, various approaches have been made to control perovskite crystallization such as sequential solution deposition [11–13], CH_3NH_3I loading time control [14], thermal interdiffusion [15], solvent annealing [16], surface property control [17, 18], retarding PbI_2 crystallization [19]. In the course of perovskite crystal formation, most of studies have put the emphasis on moisture-free environment. Decomposition or degradation of perovskite structure to precursor materials was indeed observed under humid condition [20–22]. Only a few reports addressed the effect of water during perovskite crystal formation [23–26].

In this report, we demonstrate that humidity plays a critical role to develop a thin perovskite film with controlled crystals in particular in the second spin-coating step of CH_3NH_3I on the firstly formed PbI_2 layer. As humidity increases, grains of $CH_3NH_3PbI_3$ perovskite crystals increase in size with their preferred orientation while film surface becomes roughened. Systematic investigation of device performance as a function of humidity revealed that the performance of a device of ITO/PEDOT:PSS/$CH_3NH_3PbI_3$/$PC_{71}BM$/LiF/Al was optimized in 40% relative humidity due to the two counter-acting effects on film formation. The maximum energy conversion efficiency of approximately 12% was obtained in the condition, more than 10 times greater than that of a device fabricated at 20% humidity.

2 Experimental procedures

2.1 Materials PbI_2 powder and all the chemical solvents used in this experiment were purchased from Sigma-Aldrich. CH_3NH_3I was synthesized by the process reported in the Ref. [27]. PEDOT:PSS (Clevios P VP AI4083) and $PC_{71}BM$ was purchased from Heraeus and Nano-C, respectively.

2.2 Device fabrication A thin film perovskite solar cell device was fabricated with a configuration of ITO/PEDOT:PSS/$CH_3NH_3PbI_3$/$PC_{71}BM$/LiF/Al as following. Firstly, ITO substrate was cleaned by acetone, 2-propanol for 15 min each and UV-oxygen treatment for 15 min sequentially. PEDOT:PSS was spin-coated onto the ITO substrate and then dried at 120 °C for 20 min. PbI_2 solution (460 mg/ml, DMF) was spin-coated onto PEDOT:PSS film at 3000 rpm for 15 s in N_2-filled glove box. PbI_2 solution and PEDOT:PSS substrate was cooled to room temperature before PbI_2 spin-coating. For the formation of $CH_3NH_3PbI_3$, PbI_2 substrate was brought to a humidity control chamber and CH_3NH_3I solution (38 mg/ml, 2-propanol) was spin-coated onto PbI_2 film at 4000 rpm for 30 s in different humidity conditions (except for humidity, other conditions such as the amount of oxygen were ambient condition). Its color was immediately changed to dark brown as soon as CH_3NH_3I solution was dropped on the film due to a fast reaction between CH_3NH_3I and PbI_2. A 300 nm thin film was formed. In some cases, thermal annealing was applied on perovskite film at 100 °C for 45 min in a humidity control chamber at 40 ± 3% humidity. After then, $PC_{71}BM$ (25 mg/ml, chlorobenzene) was spin-coated at 1000 rpm in N_2-filled glove box and a device fabrication was completed with the deposition of 0.9 nm LiF and 100 nm Al by thermal evaporation in high vacuum ($<6 \times 10^{-6}$ Torr). The area of active layer was defined as the crossover region between ITO and Al (0.9 cm^2). The device was sealed with an encapsulation glass using UV-curable epoxy resin with a getter film in N_2-filled glove box.

2.3 Measurement Current-density–voltage (J–V) characteristics of the devices were measured under simulated light from 1000 W xenon lamp (Oriel, 91193) of Sun 2000 solar simulator (Abet Tech.). NREL-calibrated Si solar cell (PV Measurements Inc.) was used to set the light intensity of 1-Sun (AM1.5G, 100 mW/cm^2). Optical absorbance spectra were acquired by using UV–Vis-NIR spectrometer (lambda 750, Perkin Elmer). Photoluminescence (PL) spectra were obtained using LS 55 fluorescence spectrometer (Perkin Elmer) with excitation at 480 nm.

2.4 Film characterization Surface morphology was analyzed by using field emission scanning electron microscopy (SEM, LEO 1550 VP). Atomic force microscopy (AFM) was used to obtain topography of perovskite films. Optical microscopy with Olympus BX 51M was used to visualize the perovskite films. X-ray diffraction (HR-XRD) patterns were collected at a rate of 3°/min using Rigaku SmartLab HR-XRD equipment. Grazing incidence wide angle X-ray scattering (GIWAXS) study was performed in 3C beamline in Pohang Acceleration Laboratory in Pohang, Republic of Korea. All the perovskite crystal films were fabricated on PEDOT:PSS on SiO_2 substrate and measured at the surface critical angle (error range of ±0.02°).

3 Results and discussion Figure 1a shows the two-step fabrication process we employed for high performance solar cell device involving sequential spin-casting. First, a deep yellowish PbI_2 film was formed on PEDOT:PSS/ITO/glass by spin-coating PbI_2 dissolved in DMF in N_2-filled chamber (see Fig. S1 in the Supporting Information, named SI in the following). A thin $CH_3NH_3PbI_3$ perovskite crystal film was developed on the PbI_2 surface by subsequently spin-coating CH_3NH_3I (MAI) solution dissolved in 2-propanol in the humidity control chamber without substrate heating or loading time control. During MAI spin-coating, the humidity was precisely monitored using humidity sensor (a margin of error of ±3%) from 20% relative humidity of dry condition to 80% of the maximum wet condition. Notably, optical properties

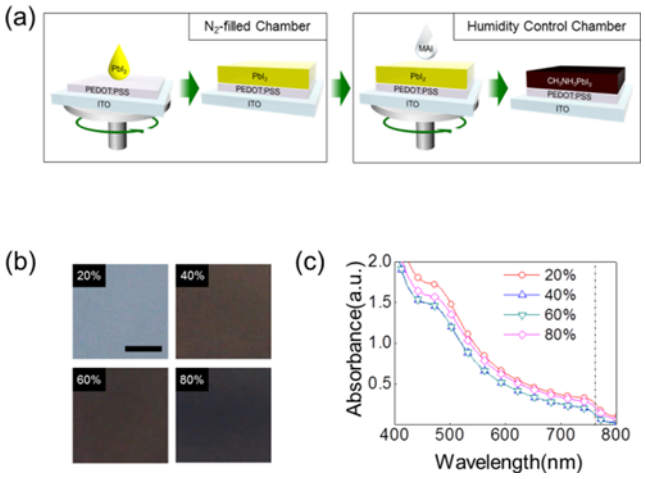

Figure 1 (a) Fabrication process of sequentially two-step spin-coated perovskite ($CH_3NH_3PbI_3$) film using a humidity control chamber. (b) Visible colors of $CH_3NH_3PbI_3$ films after MAI spin-coating in 20%, 40%, 60% and 80% humidity conditions. Scale bar is 2 mm. (c) Absorbance spectrum of $CH_3NH_3PbI_3$ films after MAI spin-coating in 20, 40, 60 and 80% humidity conditions.

of perovskite films were significantly altered, depending upon the humidity as shown in Fig. 1b. Absorbance spectra of the perovskite films processed at different humidity conditions in Fig. 1c show that the characteristic absorbance at the wavelength of 760 nm arising from band edge absorption was rarely changed. The slight variation in absorbance intensity is attributed to the perovskite films with different thickness. The results clearly suggest that there is no decomposition or transmutation of the perovskite film due to moisture and the colors of the films as a function of humidity arise from different surface scattering on the films with different microstructures as shown next.

The humidity in the second MAI spin-coating step on PbI_2 film was critical on the morphologies of perovskite crystals as shown in Fig. 2. The humidity dependent microstructures of the films were evidenced by both SEM and AFM in 3-dimensional topography mode. At relatively dry 20% humidity, exceedingly rough film with agglomerated grains of $CH_3NH_3PbI_3$ perovskite crystals was developed possibly due to the extremely fast reaction between MAI and PbI_2 (Fig. 2a and e). The morphology of a film was significantly changed when the humidity increased. For

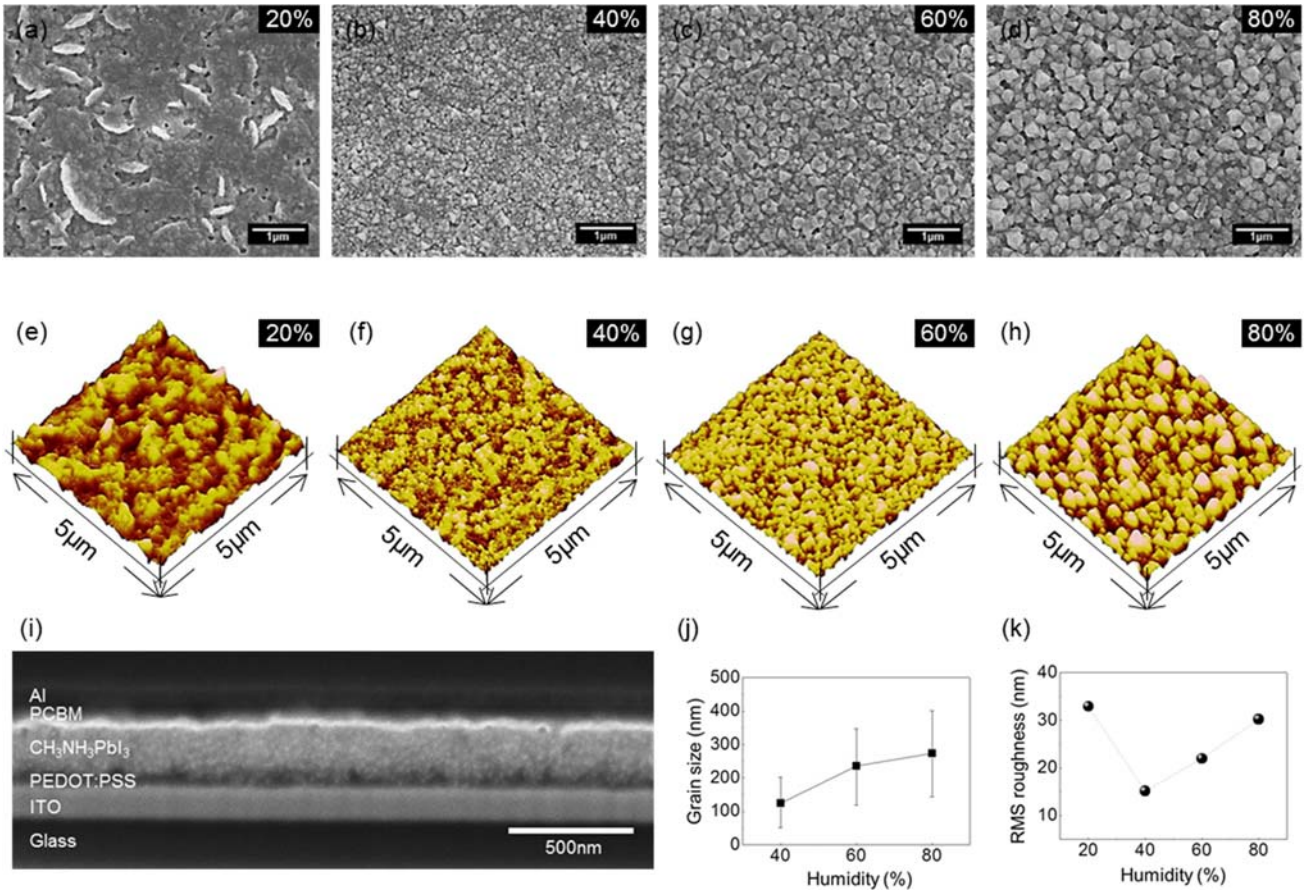

Figure 2 (a–d) SEM images of surface morphology of $CH_3NH_3PbI_3$ crystal films after MAI spin-coating in 20%, 40%, 60% and 80% humidity conditions. Scale bar is 1 μm. (e–h) 3-dimensional AFM topographic images of $CH_3NH_3PbI_3$ films after MAI spin-coating in 20%, 40%, 60% and 80% humidity conditions. (i) Cross-section SEM image of perovskite thin film fabricated in 40% humidity. (j) Average grain sizes extracted from the images (b) to (d). (k) Root mean square (RMS) roughness calculated from the images (e) to (h).

instance, a perovskite film prepared at 40% humidity was very smooth with its root-mean-squared (RMS) roughness of approximately 15 nm and exhibited very fine crystals uniformly formed with the size of approximately dozens of nanometers, as shown in Fig. 2b, f and j. Both the average grain size of perovskite crystals and the surface roughness of the films increase with the humidity as shown in Fig. 2j and k, respectively. The increased crystals with humidity can be explained by the effective crystal growth mediated by water molecules which are accumulated in the regions of crystal grain boundaries arising from the strong hygroscopic nature of MAI. The previous studies suggest that the enlarged crystals are attributed to the grain boundary creep due to water molecules within grain boundaries, followed by the effective merge of the adjacent crystals [23]. On the other hand, 3-dimensional growth of crystals in a film makes the film surface more and more rough when the average size of crystals becomes larger with humidity as shown in Fig. 2k.

The crystalline structures of the humidity dependent perovskite films were further investigated by HR-XRD as shown in Fig. 3. All the diffraction patterns of the films prepared at different humidity conditions in Fig. 3a exhibit the representative characteristic (110) reflection at 2-theta of 14.1° of tetragonal I4/mcm crystalline structure [28] while the reflection was absent in a PbI_2 film, which implies the successful formation of perovskite films during the MAI spin-coating step. It should be noted that there exist some residual PbI_2 even after the reaction with MAI as evidenced by the presence of (100) reflection of PbI_2 but the actual intensity of the reflection is more than 10 times lower than that of a pure PbI_2 film. SEM cross-section image also reveals that the crystallization occurred through the vertical direction of the film and PbI_2 residuals were rarely observed (Fig. 2i). In addition, the hydration of $CH_3NH_3PbI_3$ to $(CH_3NH_3)_4PbI_6 \cdot H_2O$ during MAI spin-coating did not happen in our system due to the absence of 7.93°, 8.42°, 10.46°, and 16.01° peaks [20]. The results suggest that humidity in our system is rarely detrimental and no degradation or decomposition of the perovskite film occurred upon sequential MAI spin-coating process. Although the crystalline structure of $CH_3NH_3PbI_3$ is all developed in the films, regardless of the humidity, it is apparent that the intensities of some of reflections are varied as a function of humidity as shown in Fig. 3a. Notably, the (110) reflection decreases with humidity whereas the (202) reflection increases, which indicates that the orientation of the perovskite crystals was affected by the humidity during the crystallization.

The humidity controlled perovskite films were further examined by GIWAXS as shown in Fig. 3b. 2-dimensional GIWAXS patterns including both out-of-plane and in-plane scattering clearly exhibit that highly ordered crystalline perovskite structure was developed when a film was crystallized in humid condition. A perovskite film prepared at nearly 0% humidity condition (H_2O level less than 1 ppm.) shows discrete ring shape reflections arising from polycrystalline tetragonal I4/mcm structure with the crys-

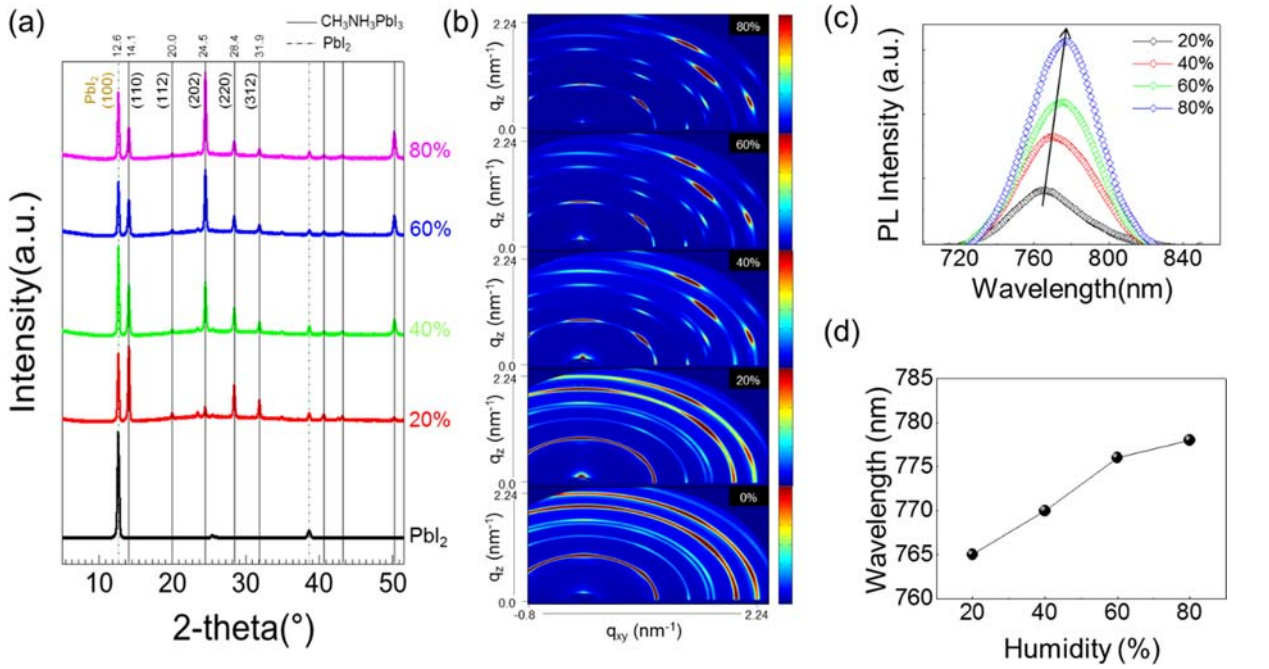

Figure 3 (a) HR-XRD patterns of PbI_2, $CH_3NH_3PbI_3$ sequentially spin-coated in 20%, 40%, 60% and 80% humidity conditions. Diffraction intensity of PbI_2 is reduced 10-times for the comparison with the $CH_3NH_3PbI_3$ films. The intensity scale of each $CH_3NH_3PbI_3$ film is represented as measured. (b) GIWAXS patterns of $CH_3NH_3PbI_3$ films sequentially spin-coated in 20%, 40%, 60% and 80% humidity conditions. (c) Photoluminescence spectra of perovskite thin films fabricated in 20%, 40%, 60% and 80% humidity and (d) peak wavelength variation (right).

tals randomly oriented [29–31]. When the humidity increases in the MAI spin-coating step, the spot-like reflections appear in particular with the humidity greater than approximately 40% above which the shape and position of the reflection were rarely changed as shown in Fig. 3b. The azimuthal plots at $q = 1.0$ nm^{-1} of the humidity controlled perovskite films again show the formation of highly oriented crystals with the humidity (Fig. S2, SI).

Both SEM and X-ray results suggest that each crystalline domain developed with humidity is nearly single crystalline with the preferred crystal orientation with respect to the substrate. In addition, these crystals were properly aggregated with each other in a way to minimize the crystal orientation mismatch at numerous grain boundaries between two domains. At high humidity, individual single crystal domains became larger and larger due to the effective retardation of crystallization by water and the large crystals assembled on a substrate made a film surface very rough. It should be noted that the grains at 0% cannot be, however, directly compared with those at 40%. As noted in the GIXD results of Fig. 3b, crystals in a film prepared at 0% humidity are randomly oriented, characterized by the presence of ring shape X-ray reflections. On the other hand, a sample at non-zero humidity contains the crystals preferentially aligned to specific directions, characterized with spot-like reflections in Fig. 3b. The different crystalline structure in a sample at 0% humidity made us avoid the direct comparison of the physical properties of the sample with those of others treated in non-zero humidity conditions.

The change in crystalline property of a thin perovskite film with humidity could also be examined with PL measurement. Not only the PL intensity increases but also the wavelength at the maximum intensity red-shifts with humidity as shown in Fig. 3c, d. A film with large single crystalline perovskite grains reduced non-radiative recombination channels arising from traps or defects, compared with one with polycrystalline grains developed at low humidity, leading to the enhanced PL intensity (Fig. 3c). The red-shift in PL peak as increasing humidity was also observed, consistent with the previous studies (Fig. 3d) [30, 32]. The single crystalline nature of a perovskite film with the minimized crystal-to-crystal mismatch at the grain boundaries can facilitate the carrier transport through the perovskite film to the corresponding electrodes, leading to high performance solar energy conversion in a device as shown next.

In order to examine the effect of the humidity controlled $CH_3NH_3PbI_3$ perovskite film on photovoltaic performance, we fabricated planar heterojunction photovoltaic device as schematically shown in Fig. 4a. For facile hole extraction to bottom ITO electrode, a hole transport layer of PEDOT:PSS was employed on which each $CH_3NH_3PbI_3$ film was developed in different humidity conditions. An electron transporting $PC_{71}BM$ layer was subsequently spin-coated, followed by the thermal evaporation of a top electrode of Al with LiF. Figure 4b shows *J–V* characteristics of solar cells with the humidity controlled $CH_3NH_3PbI_3$ films tested under the illumination of 1-Sun simulated light (AM 1.5G, 100 mA/cm^2). The results clearly show that the device performance was affected by the humidity and the performance was significantly enhanced due to the humidity up to 40% above which the device was deteriorated. Notably, a device with 40% humidity treated perovskite film exhibits its maximum power conversion efficiency (PCE) of approximately 9.37%, a short-circuit current density (J_{SC}) of 14.29 mA/cm^2, an open-circuit voltage (V_{OC}) of 0.90 V and a fill factor (FF) of 0.72. On the other hand, the devices with $CH_3NH_3PbI_3$ films prepared at 20%, 60% and 80% humidity show their PCE of 0.41%, 3.97% and 0.88%, respectively as shown in Fig. 4f. It should be noted that a device fabricated at nearly zero humidity also shows its low PCE of approximately 2.3% in our system. The reason of rather high PCE of the device, compared with that of a device prepared at 20% humidity may be due to its surface much smoother than that of 20% humidity device (Fig. S3, SI). Efficiency parameters determining PCE such as J_{SC}, V_{OC} and FF as a function of humidity in Fig. 4c–e, respectively display that the humidity dependent behavior of the devices was similar to that of PCE and a device with 40% humidity treated perovskite film showed the best performance in all the parameters. The detailed properties of the devices are summarized in Table 1 (see Supporting Information).

The humidity dependent device performance in Fig. 4 combined with the morphological results (Figs. 2 and 3) indicates that there must be a trade-off in PCE between ordering of the crystals and surface roughness. The single crystalline nature of perovskite domains arising from moisture is obviously beneficial for facile photon absorption and transport in a domain. Furthermore, the PCE becomes higher with the larger domains because grain boundaries and defects in the inter-domain regions that serve as effective recombination sites of the photo-generated carriers are reduced with the domain size. On the other hand, the roughened surface of a perovskite film is detrimental and can cause numerous leakage paths, making the shunting resistance low. Since both size of single crystalline domains and roughness of a film increases with the humidity, it is true that an optimized humidity condition should exist and the best efficiency was observed at 40% humidity.

Further improvement of a device performance was made by the post annealing process in which a device with a $CH_3NH_3PbI_3$ film two-step spin-coated in humidity condition was kept in 40% humidity condition and annealed at 100 °C for 45 min. The thermal annealing indeed increased J_{SC}, giving rise to the improved solar cell efficiency of the device as shown in Fig. S4, SI. For comparison, the devices with $CH_3NH_3PbI_3$ films prepared at different humidity of 20%, 60% and 80% were also thermally annealed. In all the cases, PCE values of the devices were enhanced with the thermal annealing but the tendency of PCE as well as J_{SC}, V_{OC} and FF as a function of humidity with the opti-

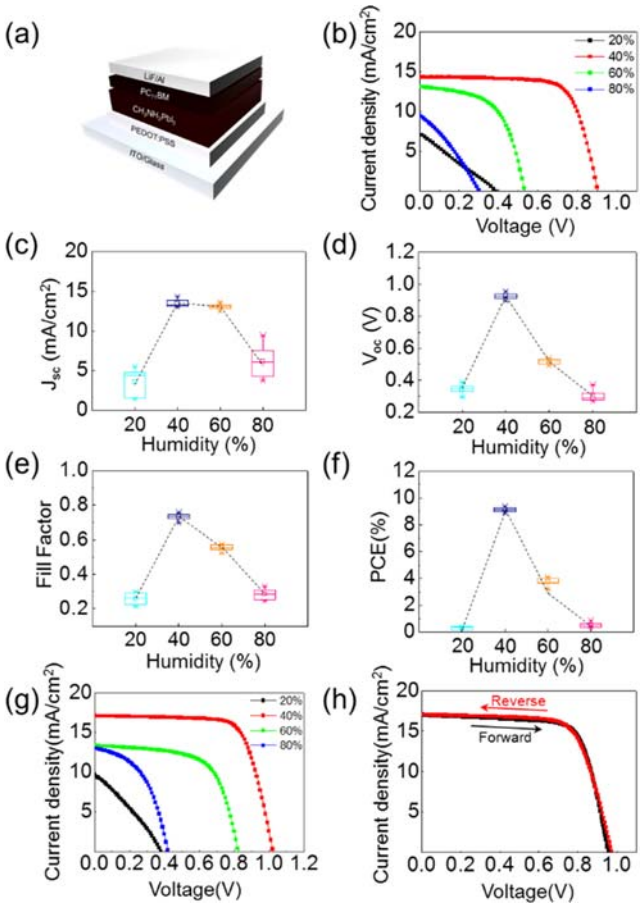

Figure 4 (a) Device architecture of $CH_3NH_3PbI_3$ solar cell tested in this study. (b) *J–V* characteristics of $CH_3NH_3PbI_3$ solar cell under 1-Sun (AM 1.5 G, 100 mW/cm^2) illumination as a function of humidity in MAI spin-coating step. (c) Box-whisker plot of short-circuit current density, (d) open-circuit voltage, (e) fill factor and (f) power conversion efficiency of $CH_3NH_3PbI_3$ solar cells as a function of humidity in MAI spin-coating step. 10 cells were tested for this study. (g) *J–V* characteristics of $CH_3NH_3PbI_3$ solar cells of MAI as-spun with different humidity conditions followed by thermal annealing in 40% humidity and (h) reverse and forward measured *J–V* curves of 40% humidity device.

mum efficiency at 40% humidity does not change as shown in Figs. 4g and S5 (SI). We also fabricated a device with a film fabricated at nearly zero humidity and approximately 6.5% PCE was obtained after thermal annealing (Fig. S3, SI). Considering that the microstructure of a perovskite film was not significantly altered after thermal annealing (Figs. S6–7, SI) but increasing the peak of perovskite (110) while decreasing PbI_2 (100) peak (Fig. S8, SI) we speculate that the increased portion of perovskite phase after thermal annealing led to the enhanced photocurrent. Incident photon-to-current efficiency measurement also reveals that the device fabricated in 40% humidity shows the best performance (Fig. S9, SI). Impedance spectra measured at $V \sim V_{OC}$ indicate that effective charge transfer occurs in the device fabricated in 40% humidity (Fig. S10, SI) [33].

It may be problematic to investigate the humidity dependent device performance even with the residual PbI_2 arising from incomplete formation of the perovskite films. However, the amount of PbI_2 in the samples after the second spin-coating in the different humidity conditions is marginal, compared with that of a pure PbI_2 film and more importantly, is all similar irrespective of the humidity conditions. The large variation in crystalline structure and the resulting device performance dependent upon humidity clearly suggests the importance of the humidity in the fabrication step.

The device fabricated at the optimized conditions of MAI spin-coating in 40% humidity and subsequent thermal annealing shows J_{SC} = 17.10 mA/cm^2, V_{OC} = 1.02 V, FF = 0.73, resulting in the best PCE of approximately 12.73%. It should also be noted that our high performance solar cell with humidity controlled perovskite film not only exhibits hysteresis-free *J–V* behavior [34] regardless of the measuring direction (Fig. 4h) but also shows remarkably low cell-to-cell variation in photovoltaic parameters as confirmed with the box-whisker plots of the parameters from 10 cells as shown in Fig. S11 (SI). We also tested the effect of the scan rate on the device hysteresis with the three different scan rates of 5, 40, 100 mV/s. No prominent hysteresis was observed with the scan rates as shown in Fig. S12 (SI). In addition, the device performance was not significantly varied with time regardless of the humidity conditions. The stability results of our encapsulated devices prepared at different humidity conditions are shown in Fig. S13 (SI). Our work mainly claims that the performance of a perovskite solar cell is affected by humidity even before thermal annealing due to the preferred crystals developed during the second spin-coating step of MAI. The post thermal annealing further increases the degree of crystallinity but the trend of the humidity dependent device performance was not altered. It is true that our solar cell efficiency values are rather low, compared with the highest world record of approximately 21%. Our results are, however, very comparable with those reported in the previous works which have successfully addressed the crystallization of perovskite materials strongly dependent upon humidity, solvent and thermal treatment as shown in Table S2 (SI) and sufficiently reliable to address the humidity effect on perovskite crystallization with low cell-to-cell variation.

4 Conclusions We demonstrated that the humidity employed in the spin-coating step of MAI on pre-formed PbI_2 film was one of the most critical factors for high performance perovskite solar cells. Our results clearly show that single crystalline domains with the minimized crystal-to-crystal mismatch at the grain boundaries are readily developed and their size becomes larger and larger while the surface of a perovskite film was roughened with the humidity. These two counter-balanced factors significantly

affected by the humidity compete with each other, giving rise to an optimum humidity (40%) condition in which the maximum PCE of approximately 9.37% was obtained. Post-annealing step following the humidity controlled spin-coating further improved the device performance. A thermally annealed device prepared at 40% humidity was rarely dependent upon voltage sweep direction, giving rise to a hysteresis-free *J–V* operation and exhibited its PCE of approximately 12.73% with very low cell-to-cell variation of 1.5%.

Supporting Information Additional supporting information may be found in the online version of this article at the publisher's website.

Acknowledgements This research was supported by the third Stage of the Brain Korea 21 Plus Project in 2014 and National Research Foundation of Korea (NRF) grant funded by the Korea government (MEST) (No. 2014R1A2A1A01005046), the Pioneer Research Foundation of Korea funded by the Ministry of Science, ICT & Future Planning (2010-0019313) and Global Ph.D. Fellowship Program through the National Research Foundation of Korea (NRF) funded by the Ministry of Education (NRF-2013H1A2A1033524).

References

[1] G. Xing, N. Mathews, S. Sun, S. S. Lim, Y. M. Lam, M. Grätzel, S. Mhaisalkar, and T. C. Sum, Science **342**, 344 (2013).
[2] D. Shi, V. Adinolfi, R. Comin, M. Yuan, E. Alarousu, A. Buin, Y. Chen, S. Hoogland, A. Rothenberger, K. Katsiev, Y. Losovyj, X. Zhang, P. A. Dowben, O. F. Mohammed, E. H. Sargent, and O. M. Bakr, Science **347**, 519 (2015).
[3] Q. Lin, A. Armin, R. C. R. Nagiri, P. L. Burn, and P. Meredith, Nature Photon. **9**, 106 (2015).
[4] N. J. Jeon, J. H. Noh, Y. C. Kim, W. S. Yang, S. Ryu, and I. Seok, Nature Mater. **13**, 897 (2014).
[5] P.-W. Liang, C.-Y. Liao, C.-C. Chueh, F. Zuo, S. T. Williams, X.-K. Xin, J. Lin, and A. K.-Y. Jen, Adv. Mater. **26**, 3748 (2014).
[6] K.-G. Lim, H.-B. Kim, J. Jeong, H. Kim, J. Y. Kim, and T.-W. Lee, Adv. Mater. **26**, 6461 (2014).
[7] Y. Zhao and K. Zhu, J. Phys. Chem. C **118**, 9412 (2014).
[8] M. Xiao, F. Huang, W. Huang, Y. Dkhissi, Y. Zhu, J. Etheridge, A. Gray-Weale, U. Bach, Y.-B. Cheng, and L. A. Spiccia, Angew. Chem. Int. Ed. **26**, 10056 (2014).
[9] J.-Y. Jeng, Y.-F. Chiang, M.-H. Lee, S.-R. Peng, T.-F. Guo, P. Chen, and T.-C. Wen, Adv. Mater. **25**, 3727 (2013).
[10] J.-H. Im, H.-S. Kim, and N.-G. Park, APL Mater. **2**, 081510 (2014).
[11] J. Burschka, N. Pellet, S.-J. Moon, R. Humphry-Baker, P. Gao, M. K. Nazeeruddin, and M. Grätzel, Nature **499**, 316 (2013).
[12] D. Liu and T. L. Kelly, Nature Photon. **8**, 133 (2014).
[13] J.-H. Im, I.-H. Jang, N. Pellet, M. Grätzel, and N.-G. Park, Nature Nanotechnol. **9**, 927 (2014).
[14] L. Zheng, Y. Ma, S. Chu, S. Wang, B. Qu, L. Xiao, Z. Chen, Q. Gong, Z. Wu, and X. Hou, Nanoscale **6**, 8171 (2014).
[15] Z. Xiao, C. Bi, Y. Shao, Q. Dong, Q. Wang, Y. Yuan, C. Wang, Y. Gao, and J. Huang, Energy Environ. Sci. **7**, 2619 (2014).
[16] Z. Xiao, Q. Dong, C. Bi, Y. Shao, Y. Yuan, and J. Huang, Adv. Mater. **26**, 6503 (2014).
[17] D. Zhao, M. Sexton, H.-Y. Park, G. Baure, J. C. Nino, and F. So, Adv. Energy Mater. **5**, 1855 (2015).
[18] H. Choi, C.-K. Mai, H.-B. Kim, J. Jeong, S. Song, G. C. Bazan, J. Y. Kim, and A. J. Heeger, Nature Commun. **6**, 7348 (2015).
[19] Y. Wu, A. Islam, X. Yang, C. Qin, J. Liu, K. Zhang, W. Peng, and L. Han, Energy Environ. Sci. **7**, 2934 (2014).
[20] J. A. Christians, P. A. M. Herrera, and P. V. Kamat, J. Am. Chem. Soc. **137**, 1530 (2015).
[21] B. Philippe, B.-W. Park, R. Lindblad, J. Oscarsson, S. Ahmadi, E. M. J. Johansson, and H. Rensmo, Chem. Mater. **27**, 1720 (2015).
[22] J. H. Kim, S. T. Williams, N. Cho, C.-C. Chueh, and A. K.-Y. Jen, Adv. Energy Mater. **5**, 1229 (2015).
[23] J. You, Y. M. Yang, Z. Hong, T.-B. Song, L. Meng, Y. Liu, C. Jiang, H. Zhou, W.-H. Chang, G. Li, and Y. Yang, Appl. Phys. Lett. **105**, 183902 (2014).
[24] S. R. Raga, M.-C. Jung, M. V. Lee, M. R. Leyden, Y. Kato, and Y. Qi, Chem. Mater. **27**, 1597 (2015).
[25] S. M. Seetharaman, P. Nagarjuna, P. N. Kumar, S. P. Singh, M. Deepa, and M. A. G. Namboothiry, Phy. Chem. Chem. Phys. **16**, 24691 (2014).
[26] H. Zhou, Q. Chen, G. Li, S. Luo, T.-B. Song, H.-S. Duan, Z. Hong, J. You, Y. Liu, and Y. Yang, Science **345**, 542 (2014).
[27] J.-H. Im, C.-R. Lee, J.-W. Lee, S.-W. Park, and N.-G. Park, Nanoscale **3**, 4088 (2011).
[28] T. Baikie, Y. Fang, J. M. Kadro, M. Schreyer, F. Wei, S. G. Mhaisalkar, M. Grätzel, and T. J. White, J. Mater. Chem. A **1**, 5628 (2013).
[29] K. W. Tan, D. T. Moore, M. Saliba, H. Sai, L. A. Estroff, T. Hanrath, H. J. Snaith, and U. Wiesner, ACS Nano **8**, 4730 (2014).
[30] W. Zhang, M. Saliba, D. T. Moore, S. K. Pathak, M. T. Hörantner, T. Stergiopoulos, S. D. Stranks, G. E. Eperon, J. A. Alexander-Webber, A. Abate, A. Sadhanala, S. Yao, Y. Chen, R. H. Friend, L. A. Estroff, U. Wiesner, and H. J. Snaith, Nature Commun. **6**, 6142 (2015).
[31] Y.-C. Huang, C.-S. Tsao, Y.-J. Cho, K.-C. Chen, K.-M. Chiang, S.-Y. Hsiao, C.-W. Chen, C.-J. Su, U.-S. Jeng, and H.-W. Lin, Sci. Rep. **5**, 13657 (2015).
[32] M. D. Bastiani, V. D'Innocenzo, S. D. Stranks, H. J. Snaith, and A. Petrozza, APL Mater. **2**, 081509 (2014).
[33] K. Wang, C. Liu, P. Du, H.-L. Zhang, and X. Gong, Small 11, 3369 (2015).
[34] J. H. Heo, H. J. Han, D. Kim, T. K. Ahn, and S. H. Im, Energy Environ. Sci. **8**, 1602 (2015).